Available online at www.sciencedirect.com

ScienceDirect

Scripta Materialia 81 (2014) 16–19

Scripta MATERIALIA

www.elsevier.com/locate/scriptamat

A novel approach to measure grain boundary segregation in bulk polycrystalline materials in dependence of the boundaries' five rotational degrees of freedom

S. Mandal,* K.G. Pradeep,* S. Zaefferer and D. Raabe

Max-Planck Institut für Eisenforschung, Max-Planck Str. 1, 40237 Düsseldorf, Germany

Received 19 January 2014; revised 10 February 2014; accepted 11 February 2014
Available online 20 February 2014

We demonstrate a simplified nondestructive 3-D electron backscatter diffraction (EBSD) methodology that enables the measurement of all five degrees of freedom of grain boundaries (GBs) combined with segregation analysis using atom probe tomography (APT). The approach is based on two 2-D EBSD measurements on orthogonal surfaces at a sharp edge of the specimen followed by site-specific GB composition analysis using APT. An example of an asymmetric Σ9 boundary exhibiting GB segregation emphasizes the need for complete GB characterization in this context.

Keywords: Grain boundary crystallography; Electron backscatter diffraction; Atom probe tomography; Segregation

There is considerable evidence in the literature suggesting that the segregation of solute elements at grain boundaries (GBs) largely depends on the structure and character of these boundaries [1–5]. Historically, GBs have been broadly classified into two categories, namely coincidence site lattice (CSL) boundaries and random high-angle boundaries (HAGBs). More accurately a third category, referred to as vicinal boundaries, needs to be introduced, describing boundaries that deviate to a certain degree from perfect CSL boundaries [6]. CSL boundaries are often assumed to be more resistant to segregation compared to random HAGBs. Grain boundary engineering has been employed in the past to enhance the resistance of materials to segregation [7,8]. The majority of these studies are based on the objective of increasing the proportions of low Σ (Σ⩽29) CSL boundaries as these are often considered as low-energy "special boundaries" (SBs). This is, however, an over-simplification. A GB is crystallographically defined by five rotational degrees of freedom (DOFs). Three independent parameters are required to describe the misorientation between grains (e.g. two DOFs for the misorientation axis and one for the misorientation angle), while the remaining two independent parameters describe the orientation of the GB plane. Since the value of Σ represents only the mutual misorientation of two adjoining crystal lattices, it does not provide any information on the orientation of the GB plane and the degree of coherency in it. Due to these shortcomings, the CSL model fails in correctly classifying GBs (i.e. SBs or random) in many situations [9,10]. This emphasizes that the occurrence of a certain coincidence lattice is not a sufficient criterion for a GB to be special.

This means that the GB plane should also be considered along with the misorientation when defining a GB as "random" or "special". Consequently, the concept of "grain boundary plane engineering" has recently been suggested [11]. However, experimental data correlating the five-parameter GB character and properties (e.g. segregation) has rarely been reported. This is attributed to the fact that metallographic techniques often applied for the characterization of microstructures are on 2-D surfaces, which allows a maximum of four parameters to be determined, namely the misorientation (three parameters) and the trace vector of the boundary on the surface (one parameter). If a sufficiently large number of GBs in an equilibrated microstructure is studied, a stereological technique enables one to quantify the five-parameter grain boundary distribution from 2-D observations [12]. However, such measurement provides information about the statistical distributions of planes, but not for specific boundaries. Although it is possible to determine all five DOFs of a GB by employing 3-D electron backscatter diffraction (EBSD) [13,14] of serial

* Corresponding authors. Tel.: +49 211 6792 949; fax: +49 211 6792 333; e-mail addresses: sumantra.igcar@gmail.com; kgprad@gmail.com

http://dx.doi.org/10.1016/j.scriptamat.2014.02.016
1359-6462/

sections, this method is destructive and hence cannot be utilized to study the properties of the investigated boundaries, e.g. composition, which requires the use of atom probe tomography (APT). One approach to determine all five DOFs of a GB while preserving its structure is to employ transmission electron microscopy (TEM) on an APT microtip [15]. However, determination of the complete crystallography of internal interfaces by TEM is generally a complex and tedious procedure. Recently, Baik et al. [16] have combined EBSD and focused ion beam (FIB) to characterize a GB's five DOFs and subsequently performed APT to determine GB composition. Alternatively, here we propose a "pseudo" 3-D EBSD approach for measuring all five DOFs of GBs while preserving the boundaries for subsequent APT analysis. The methodology is based on the 2-D EBSD measurement on two orthogonal surfaces of "sharp edge" rectangular specimens (Fig. 1a). The approximate areas of interest near the sharp edge "XY" are marked by the dotted red lines. On each of these two surfaces a trace belonging to the same GB can be determined from which the boundary plane can be evaluated. The concept of determining the GB plane orientation from observations on orthogonal sections was first suggested by Randle [17]. The approach requires that the GB segment be reasonably flat close to the edge. Such a measurement strategy essentially allows us to obtain the GB misorientation as well as the GB traces on the two orthogonal directions. From these measurements, all five DOFs of those boundaries intersecting the edge can be evaluated. Site-specific APT analyses of the pre-characterized GBs can be carried out to estimate how the GB segregation depends on the five DOFs.

The material studied here is an austenitic stainless steel type 304L containing Fe–17.6Cr–13.7Ni–0.017C–0.089P–0.025Mn–0.003S–0.01Si–0.0045N–0.0028Co (all in wt.%). A large amount of P was added intentionally to produce pronounced GB segregation. To homogenize the steel, hot rolling (thickness reduction from 60 to 6 mm) at 1373 K was performed on the as-cast material. The hot-rolled plate was subsequently solution-annealed at 1323 K for 60 min followed by water quenching to room temperature. Long-term annealing (at 923 K for 100 h) was performed to promote strong equilibrium segregation of P. Specimens for GB determination were prepared by standard mechanical grinding and polishing procedures with a 50 nm colloid suspension of SiO_2 as a final polishing step. Extreme care was taken during polishing to preserve and prepare a "sharp edge" (edge radius <0.5 μm). EBSD scans were performed on orthogonal surfaces of the sharp edge with a Zeiss XB1540 microscope, using a step size of 0.5 μm at an electron beam accelerating voltage of 15 kV. The collected EBSD data were analyzed using TSL OIM 6.2 analysis software. For identifying CSL boundaries, Brandon's criterion was used [18]. Site-specific lift out was carried out on pre-characterized (with respect to all the five DOFs) boundaries along the sample edge using a dual-beam FIB (FEI Helios NanoLab™ 600*i*). APT was performed with a local electrode atom probe (LEAP™ 3000X HR, Cameca Instruments) in voltage mode at ~60 K. The pulse fraction and repetition rates employed were 15% and 200 kHz, respectively [19]. Data reconstruction and analysis was carried out using IVAS 3.6.6 software.

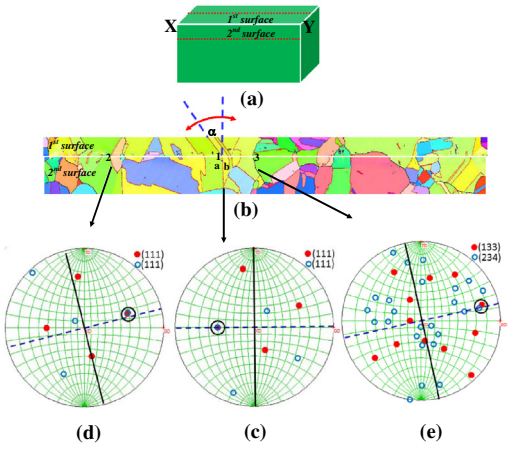

Figure 1. (a) Schematic illustration of a "sharp edge" specimen showing the approximate location (by red dotted line) where EBSD measurements were carried out. (b) Two IPF maps (with the sample edge direction as common reference direction) for the two mutual perpendicular surfaces near the sharp edge (boundary color code: Σ3, red; Σ9, blue; other HAGBs, black). (c–e) Stereographic projections for three representative GBs displaying the two abutting crystals, the boundary traces (black lines) and potential boundary normals (dashed blue lines); filled red circles and open blue circles in (c–e) represent all the potential symmetrically equivalent planes from the 1st and 2nd crystals, respectively, whereas the open black circle indicates the actual boundary plane. (For interpretation of the references to colour in this figure legend, the reader is referred to the web version of this article.)

Figure 1b shows the inverse pole figure (IPF) maps displaying the crystallographic direction parallel to the edge direction of the sample of the two mutually perpendicular surfaces (denoted as the 1st and 2nd surface, respectively) near the sharp edge. The boundary traces on both surfaces were identified from the IPF maps. A graphical procedure to evaluate the boundary plane of individual GBs is explained in the following. The plane of boundary 1 (which is likely to be a coherent twin boundary as it has straight traces, see Fig. 1b) is evaluated first. The boundary has a misorientation of 59.6°<1 1 −1> and deviates by 0.4° from the exact Σ3 relationship as per Brandon's criterion. The orientations of the two neighbouring face-centered cubic crystals of the boundary 1 (i.e. crystals a and b in the lower IPF of Fig. 1b) are plotted in a stereographic projection (Fig. 1c). The trace of the boundary from the IPF map of the 2nd surface is plotted onto the stereographic projection as a black line (Fig. 1c). Since the boundary plane normal is perpendicular to its trace, it is obvious that the plane normal of boundary 1 lies somewhere along the dashed blue line (Fig. 1c). In addition, the inclination of the boundary plane is measured on the 1st surface to evaluate the exact position of the boundary plane normal. The vertical inclination angle of the boundary trace in the IPF map of the 1st surface (i.e. the angle α, see Fig. 1b) is measured to be 40°. This indicates that the boundary plane normal lies 40° away from the X-reference axis (as shown by the open black circle in Fig. 1c) which overlaps exactly (with <1° deviation) with the superimposing (1 1 1) poles from both adjoining crystals. Hence, the Miller indices of boundary 1 are (1 1 1) for both grains as highlighted in the stereograph (Fig. 1c). The results of the five-parameter study confirmed that the boundary 1 is a coherent Σ3 twin. Applying the same procedure, all five DOFs of the other boundaries were evaluated. Two representative boundaries are shown

in Figure 1d and e, respectively. Figure 1d reveals that boundary 2, which is also a Σ3 boundary (with a misorientation of 59.8° <−17 18 17> and a deviation of 1.4°), does not lie exactly on a (1 1 1) plane. The boundary plane deviates by ~3° from the ideal (1 1 1) plane. Figure 1e shows a HAGB (i.e. boundary 3 which has a misorientation of 49.2°<−15 5 17>) lying close to a high-index plane (4 2 −3) for one crystal and 2.6° away from the (−1 3 3) plane for the other crystal. It is hence identified as a random HAGB. It is worth mentioning here that the boundary plane could also be determined as follows: on both surfaces, i (i = 1,2), the crystallographic directions $[uvw]_i$ of the boundary traces under consideration are measured separately for each of the grains involved in the boundary. Note that it is important to use the same symmetry variant for the orientation measurements on the two surfaces. Furthermore, care has to be taken to keep the sense of the trace line measurement. The Miller indices of the boundary plane segment are then calculated according to Eq. (1) for each of the two crystals:

$$(hkl)_{\text{plane}} = [uvw]_1 \times [uvw]_2 \quad (1)$$

To highlight the importance of the boundary plane on categorizing a GB as "special" or "random", the segregation behaviour of a Σ9 boundary will now be presented. There exists a certain degree of ambiguity in the literature as to whether or not the Σ9 boundary should be regarded as "special" [20–23]. A Σ9 boundary is usually formed from a secondary twinning event, i.e. when a twin forms inside of a twin. The boundary of this second twin with respect to the original parent has Σ9 character. The Σ9 boundary that was investigated here (marked by an arrow in Fig. 2a) has a misorientation of 37.4°<−1 1 0> (with a deviation of 1.6° with respect to the ideal Σ9 boundary). By means of trace analysis and employing the same computer program that is used to plot the stereographic projections in this paper (TOCA [24]) it was found that the boundary in this specific case can be described best by a combination of $(125)_{\text{grain1}}/(177)_{\text{grain2}}$ planes (see Fig. 2b). The boundary planes thus have random, asymmetric character. The determined planes are calculated to be 2° off from perfect parallelism and they are by ~4° off from the experimentally determined position of the boundary normal vector.

Site-specific lift-out of APT tips was performed for this Σ9 boundary employing a dual-beam FIB. A schematic of the lift-out process is shown in Figure 3. Initially, a protective layer of ~1 μm thick platinum was deposited on the surface of the target GB as shown in Figure 3b to avoid Ga^+ ion beam damage during milling. A 20 × 4 μm^2 wedge-shaped sample containing the GB area was lifted out (see Fig. 3c–e) and slices of this wedge were mounted and glued over several pre-fabricated Si posts of 2 μm in diameter each using Pt precursor gas (Fig. 3f). The sequences of milling steps involved are shown in Figure 3g,h, where the exact GB position between grain 1 and 2 within the 2 μm sample wedge are identified prior to final milling. As the inclination angle of the boundary plane is known (from Fig. 2a) and the Pt deposition identifies locally the GB region on the wedge (Fig. 3g), all the milling steps can be precisely performed such that the GB area is retained in the APT sample. Annular milling was performed in steps of decreasing milling currents, precisely over the GB region as shown in Figure 3g. Final low-energy (5 keV) Ga^+ ion-milling was carried out to minimize beam damage and also to form a microtip of ~16 nm radius of curvature (Fig. 3h).

Figure 4 shows the 3-D elemental maps of all the constituent elements from a reconstructed volume of 43 × 43 × 90 nm^3 containing the Σ9 GB. From the individual atom maps in Figure 4a, it is obvious that P shows substantial segregation, whereas C segregates marginally. Other elements such as Fe, Ni, Cr and N do not show any preferential segregation. The GB region could also be distinguished in terms of a 0.4 at.% P isoconcentration surface (see Fig. 4b) and the equilibrium Gibbsian interfacial excess Γ_P, was obtained using a 1-D concentration depth profile (in Fig. 4c). For this purpose a cylindrical region of interest with 5 nm radius was oriented perpendicular to the direction of the GB plane and the concentration–depth profiles were plotted with a bin size of 0.8 nm along the depth direction of the cylinder as shown in Figure 4b. The concentration profile reveals a strong segregation of

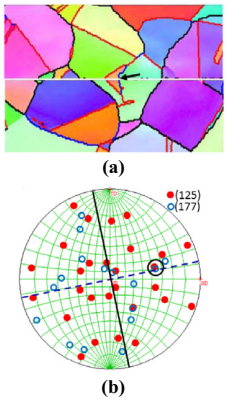

Figure 2. (a) IPF maps of the two mutual perpendicular surfaces near the sharp edge showing a Σ9 boundary (boundary color code: same as in Fig. 1b). (b) Stereographic projections displaying the normals of the (1 2 5) planes of the first crystal and the (1 7 7) planes of the second crystal. The boundary trace is plotted as a black line; the potential boundary normals are on the blue line. (For interpretation of the references to colour in this figure legend, the reader is referred to the web version of this article.)

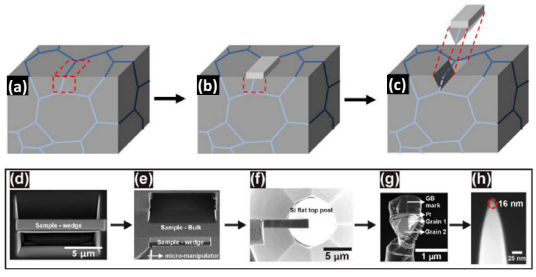

Figure 3. Precision site-specific FIB-based sample preparation procedure for preparing APT tips: (a) selected GBs based on EBSD measurements on orthogonal surfaces near a sharp edge; (b) protective Pt layer deposition; (c) wedge-shaped sample (20 × 4 μm^2) is lifted out from the selected GB region with Pt as reference employing the following sequences: (d) SEM image of the wedge after milling along the GB area; (e) wedge connected to the micromanipulator needle and lifted out; (f) sampling over pre-fabricated Si flat-top posts by milling and Pt welding; (g) identification of GB region from the grain orientation contrast and line marking for final annular milling; (h) final sharp APT microtip containing the desired GB.

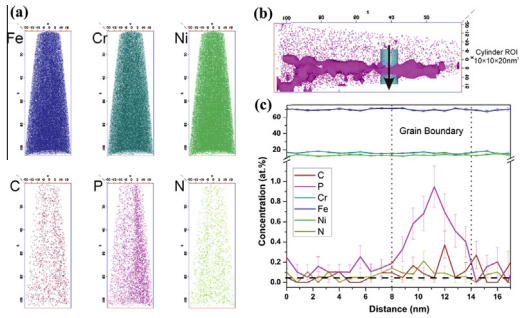

Figure 4. (a) 3-D reconstruction of individual atom positions showing enrichment of P atoms along the GB. (b) Boundary region defined using a 0.4 at.% P isoconcentration surface. (c) The concentration profiles for each atomic species obtained using a cylinder of 5 nm radius for the Σ9 boundary.

P over a distance of 6 nm with a peak concentration of ~1 at.%.

According to the Gibbs adsorption isotherm [25]:

$$d\gamma = -\Gamma_P d\mu_P \quad (2)$$

where γ is the GB energy, Γ_P is the excess of P atoms in the boundary and μ_P is the chemical potential of P. This equation relates the change of GB energy to the equilibrium interfacial excess of P atoms (N_P) per unit area [25]. In this work the Γ_P was calculated from the 1-D concentration profile (see Fig. 4c) by subtracting the matrix (or grain interior) concentration from the measured concentration of P across the GB [26]. Accordingly, the calculated value of Γ_P for the Σ9 GB was 2.85 ± 0.1 atoms nm^{-2}, indicating substantial P segregation. The total reduction in interfacial energy, γ, as a result of P segregation was estimated to be 857.81 ± 31.48 mJ m^{-2} from Eq. (2) by employing the calculated Γ_P and the concentration of P in the matrix as described in Refs. [16,27]. Experimental observation clearly indicates that the reduction in γ due to P segregation along the Σ9 boundary is substantial and comparable to that of a random HAGB [16]. The present study also reveals that the investigated Σ9 GB, in spite of being a low Σ CSL boundary, does not exhibit "special" behaviour regarding its resistance to segregation. This is attributed to the fact that the studied Σ9 boundary is not symmetric, i.e. the Miller indices of the boundary plane measured with respect to the two mutual grains are not identical and, therefore, also do not correspond to a coherency plane (Fig. 2b). It has been supposed earlier that Σ9 boundaries do not exhibit any energetic preference [20,28] and that their large fraction in low stacking fault energy materials is essentially due to the geometric connection between Σ3 boundaries during the multiple twinning process [22,28,29]. The present result agrees well with this supposition.

In summary, a novel approach for measuring all five DOFs of GBs by EBSD while preserving the same for subsequent APT analysis to determine the segregation behaviour has been suggested in this study. Two sets of 2-D EBSD measurements on orthogonal surfaces of a "sharp edge" specimen provide the necessary crystallographic details on GBs, whereas the site-specific APT analysis of pre-characterized GBs allows us to measure interfacial segregation. To highlight the importance of measuring all five DOFs for categorizing a GB as "special" or "random", segregation on a Σ9 boundary in a P-doped 304L steel has been presented. It has been shown that P segregates substantially and the total reduction in interfacial free energy due to P segregation was 857.81 ± 31.48 mJ m^{-2}. This indicates that the investigated Σ9 GB does not exhibit a "special" behaviour which has been attributed to the fact that the studied Σ9 GB plane has a random, asymmetric character. The results underline the need for a comprehensive GB characterization in terms of crystallography and chemistry in order to understand the GB properties, which in turn determine the overall material performance.

The authors thank Daniel Haley for valuable discussions. The authors are also grateful for the support of the Alexander von Humboldt Foundation.

[1] T. Ogura, T. Watanabe, S. Karashima, T. Masumoto, Acta Metall. 35 (1987) 1807.
[2] T.S. Duh, J.J. Kai, F.R. Chen, L.H. Wang, J. Nucl. Mater. 258–263 (1998) 2064.
[3] P. Lejcek, S. Hofmann, V. Paidar, Acta Mater. 51 (2003) 3951.
[4] M.L. Taheri, J.T. Sebastian, B.W. Reed, D.N. Seidman, A.D. Rollett, Ultramicroscopy 110 (2010) 278.
[5] M. Tomozawa, Y. Miyahara, K. Kako, Mater. Sci. Eng., A 167 (2013) 578.
[6] A.P. Sutton, R.W. Balluffi, Acta Metall. 35 (1987) 2177.
[7] M. Kurban, U. Erb, K.T. Aust, Scripta Mater. 54 (2006) 1053.
[8] S. Kobayashi, S. Tsurekawa, T. Watanabe, G. Palumbo, Scripta Mater. 62 (2010) 294.
[9] P. Lejcek, J. Adamek, S. Hofmann, Surface Sci. 264 (1992) 449.
[10] P. Lejcek, V. Paidar, J. Adamek, S. Hofmann, Acta Mater. 45 (1997) 3915.
[11] V. Randle, Scripta Mater. 54 (2006) 1011.
[12] D.M. Saylor, B.S. El Dasher, A.D. Rollett, G.S. Rohrer, Acta Mater. 52 (2004) 3649.
[13] A.D. Rollet, S.-B. Lee, R. Campman, G.S. Rohrer, Annu. Rev. Mater. Res. 37 (2007) 627.
[14] A. Khorashadizadeh, D. Raabe, S. Zaefferer, G.S. Rohrer, A.D. Rollett, M. Winning, Adv. Eng. Mater. 13 (2011) 237.
[15] M. Herbig, D. Raabe, Y.J. Li, P. Choi, S. Zaefferer, S. Goto, Phy. Rev. Lett. (in press).
[16] Sung-Il Baik, M.J. Olszta, S.M. Bruemmer, D.N. Seidman, Scripta Mater. 66 (2012) 809.
[17] V. Randle, Mater. Charact. 34 (1995) 29.
[18] D.G. Brandon, Acta Metall. 14 (1966) 1479.
[19] H. Zhang, K.G. Pradeep, S. Mandal, D. Ponge, P. Choi, C.C. Tasan, D. Raabe, Acta Mater. 63 (2014) 232.
[20] V.Y. Gertsman, S.M. Bruemmer, Acta Mater. 49 (2001) 1589.
[21] Y. Takehara, H. Fujiwara, H. Miyamoto, Met. Mater. Trans. 44A (2013) 3685.
[22] V. Randle, R. Jones, Mater. Sci. Eng., A 524 (2009) 134.
[23] J.G. Hu, S.-M. Kuo, A. Seki, B.W. Krakauer, D.N. Seidman, Scripta Metall. 23 (1989) 2033.
[24] S. Zaefferer, Advances in Imaging and Electron Physics 125 (2002) 355.
[25] R. Kirchheim, Acta Mater. 50 (2002) 413.
[26] B.W. Krakauer, D.N. Seidman, Acta Mater. 46 (1998) 6145.
[27] D. Isheim, M.S. Gagliano, M.E. Fine, D.N. Seidman, Acta Mater. 54 (2006) 841.
[28] V.Y. Gertsman, K. Tangri, Philos. Mag. 64A (1991) 1319.
[29] S. Mandal, A.K. Bhaduri, V.S. Sarma, J. Mater. Sci. 46 (2011) 275.